

Similar evolutionary trajectories for retrotransposon accumulation in mammals

Reuben M Buckley¹, R Daniel Kortschak¹, Joy M Raison¹, David L Adelson^{1,*}

1 Department of Genetics and Evolution, The University of Adelaide, North Tce, 5005, Adelaide, Australia

* david.adelson@adelaide.edu.au

Keywords: Transposable element, Genome Evolution, Genome Architecture

Running title: Similar evolutionary trajectories in mammals

Abstract

The factors guiding retrotransposon insertion site preference are not well understood. Different types of retrotransposons share common replication machinery and yet occupy distinct genomic domains. Autonomous long interspersed elements accumulate in gene-poor domains and their non-autonomous short interspersed elements accumulate in gene-rich domains. To determine genomic factors that contribute to this discrepancy we analysed the distribution of retrotransposons within the framework of chromosomal domains and regulatory elements. Using comparative genomics, we identified large-scale conserved patterns of retrotransposon accumulation across several mammalian genomes. Importantly, retrotransposons that were active after our sample-species diverged accumulated in orthologous regions. This suggested a conserved interaction between retrotransposon activity and conserved genome architecture. In addition, we found that retrotransposons accumulated at regulatory element boundaries in open chromatin, where accumulation of particular retrotransposon types depended on insertion size and local regulatory element density. From our results, we propose a model where density and distribution of genes and regulatory elements canalise the accumulation of retrotransposons. Through conservation of synteny, gene regulation and nuclear organisation, we have found that mammalian genomes follow similar evolutionary trajectories.

Introduction

An understanding of the dynamics of evolutionary changes in mammalian genomes is critical for understanding the diversity of mammalian biology. Most work on mammalian molecular evolution is on protein coding genes, based on the assumed centrality of their roles and because of the lack of appropriate methods to identify the evolutionary conservation of apparently non-conserved, non-coding sequences. Consequently, this approach addresses only a tiny fraction (less than 2%) of a species' genome, leaving significant gaps in our understanding of evolutionary processes (Consortium et al. 2012; Lander et al. 2001). In this report we describe how large scale positional conservation of non-coding, repetitive DNA sheds light on the possible conservation of mechanisms of genome evolution, particularly with respect to the acquisition of new DNA sequences.

Mammalian genomes are hierarchically organised into compositionally distinct hetero- or

1
2
3
4
5
6
7
8
9
10
11
12

euchromatic large structural domains (Gibcus and Dekker 2013). These domains are largely 13 composed of mobile self-replicating non-long terminal repeat (non-LTR) retrotransposons; 14 with Long INterspersed Elements (LINEs) in heterochromatic regions and Short INterspersed 15 Elements (SINEs) in euchromatic regions (Medstrand et al. 2002). The predominant LINE in 16 most mammals is the ~6 kb long L1. This autonomously replicating element is responsible 17 for the mobilisation of an associated non-autonomous SINE, usually ~300 bp long. Together, 18 LINEs and SINEs occupy approximately 30% of the human genome (Lander et al. 2001), 19 replicate via a well characterised RNA-mediated copy-and-paste mechanism (Cost et al. 20 2002) and co-evolve with host genomes (Kramerov and Vassetzky 2011; Chalopin et al. 2015; 21 Furano et al. 2004). 22

The accumulation of L1s and their associated SINEs into distinct genomic regions depends 23 on at least one of two factors. 1) Each element's insertion preference for particular genomic 24 regions and 2) the ability of particular genomic regions to tolerate insertions. According to 25 the current retrotransposon accumulation model, both L1s and SINEs likely share the same 26 insertion patterns constrained by local sequence composition. Therefore, their accumulation 27 in distinct genomic regions is a result of region specific tolerance to insertions. Because L1s 28 are believed to have a greater capacity than SINEs to disrupt gene regulatory structures, 29 they are evolutionarily purged from gene-rich euchromatic domains at a higher rate than 30 SINEs. Consequently, this selection asymmetry in euchromatic gene-rich regions causes L1s 31 to become enriched in gene-poor heterochromatic domains (Lander et al. 2001; Graham and 32 Boissinot 2006; Gasior et al. 2007; Kvikstad and Makova 2010). 33

An important genomic feature, not explored in the accumulation model, is the chromatin 34 structure that surrounds potential retrotransposon insertion sites. Retrotransposons 35 preferentially insert into open chromatin (Cost et al. 2001; Baillie et al. 2011), which is 36 usually found overlapping gene regulatory elements. As disruption of regulatory elements 37 can often be harmful, this creates a fundamental evolutionary conflict for retrotransposons: 38 their immediate replication may be costly to the overall fitness of the genome in which they 39 reside. Therefore, rather than local sequence composition and/or tolerance to insertion alone, 40 retrotransposon accumulation is more likely to be constrained by an interaction between 41 retrotransposon expression, openness of chromatin, susceptibility of a particular site to alter 42 gene regulation, and the capacity of an insertion to impact on fitness. 43

To investigate the relationship between retrotransposon activity and genome evolution, 44

we began by characterising the distribution and accumulation of non-LTR retrotransposons 45
within placental mammalian genomes. Next, we compared retrotransposon accumulation 46
patterns in five separate evolutionary paths by humanising the repeat content (see methods) 47
of the chimpanzee, rhesus macaque, mouse and dog genomes. Finally, we analysed human 48
retrotransposon accumulation in large hetero- and euchromatic structural domains, focussing 49
on regions surrounding genes, exons and regulatory elements. Our results suggested that 50
accumulation of particular retrotransposon families follows from insertion into open chromatin 51
found adjacent to regulatory elements and depends on local gene and regulatory element 52
density. From this we propose a refined retrotransposon accumulation model in which 53
random insertion of retrotransposons is primarily constrained by chromatin structure rather 54
than local sequence composition. 55

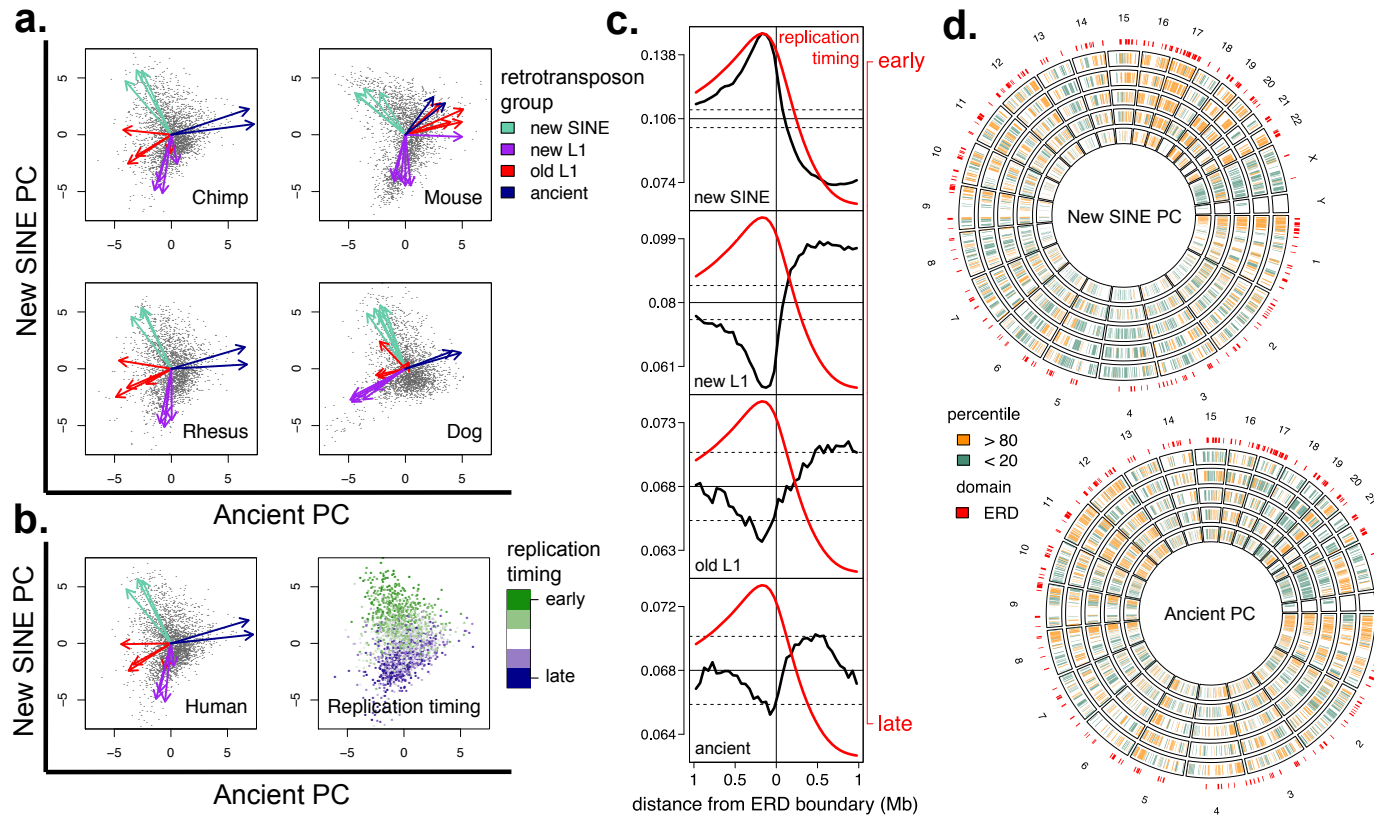


Figure 1. Large-scale genome distributions of retrotransposons are strongly associated with replication timing and conserved in distant mammalian species.

a. PCA of non-human genome retrotransposon content, each vector loading has been coloured according to the retrotransposon group it represents. PC1 and PC2 have been renamed according to the retrotransposon group whose variance they principally account for. **b.** PCA of human retrotransposon content and mean genome replication timing in HUVEC cells. **c.** Retrotransposon density per non-overlapping 50 kb intervals from a pooled set of ERD boundaries across all 16 cell lines. Black dashed lines indicate 2 standard deviations from the mean (solid horizontal black line). Red line indicates mean replication timing across all samples. **d.** 20% tails of New SINE and Ancient PC scores of humanised genomes plotted against human, large ERDs (> 2 Mb) from HUVEC cells marked in red. Species from centre are human, chimpanzee, rhesus macaque, mouse and dog.

Results

56

Species selection and retrotransposon classification

57

We selected human, chimpanzee, rhesus macaque, mouse and dog as representative placental species because of their similar non-LTR retrotransposon composition (Fig. S1-S2) and phylogenetic relationships. Retrotransposon coordinates were obtained from the UCSC repeat

58

59

60

masker tables (Rosenbloom et al. 2015; Smit et al. 1996) and non-LTR retrotransposon 61 families were grouped according to repeat type and period of activity as determined by 62 genome-wide defragmentation (Giordano et al. 2007). Retrotransposons were placed into the 63 following groups; new L1s, old L1s, new SINEs and ancient elements (for families in each 64 group see Fig. S2). New L1s and new SINEs are retrotransposon families with high clade 65 specificity and activity, while old L1s and ancient elements (SINE MIRs and LINE L2s) 66 are retrotransposon families shared across taxa. We measured sequence similarity within 67 retrotransposon families as percentage mismatch from family consensus sequences (Bao et al. 68 2015) and confirmed that our classification of retrotransposon groups agreed with ancestral 69 and clade-specific periods of retrotransposon activity (Fig. S3). 70

Genomic distributions of retrotransposons 71

To analyse the large scale distribution of retrotransposons, we segmented each species 72 genome into adjacent 1 Mb regions, tallied retrotransposon distributions, performed principal 73 component analysis (PCA) and pairwise correlation analysis (see methods). From the PCA, 74 we found that new SINEs and ancient elements strongly associated with the two major 75 principal components (PC1 and PC2). Depending on this association we identified PC1 76 and PC2 as “New SINE PC” and “Ancient PC” respectively, or the converse (Fig. 1a). 77 This showed that retrotransposon families from the same group accumulated in the same 78 genomic regions. For all species examined, new SINEs were enriched in regions with few new 79 L1s, and in all species except mouse — where ancient elements and old L1s were co-located 80 — ancient elements were enriched in regions with few old L1s (Fig. 1a, S4). This mouse 81 discordance has probably resulted from the increased genome turnover seen in the rodent 82 lineage (Murphy et al. 2005) disrupting the distribution of ancestral retrotransposon families 83 (Fig. S1-S2). As the relationship between mouse clade-specific new retrotransposons is 84 maintained, this discordance does not impact on downstream analyses. These results show 85 that most genomic context associations between retrotransposon families are conserved across 86 our sample species. 87

Retrotransposon accumulation and chromatin environment

88

In human and mouse, LINEs and SINEs differentially associate with distinct chromatin environments (Ashida et al. 2012). To determine how our retrotransposon groups associate with chromatin accessibility, we obtained cell line Repli-Seq data (Hansen et al. 2010a) from the UCSC genome browser. Repli-Seq measures the timing of genome replication during S-phase, where accessible euchromatic domains replicate early and inaccessible heterochromatic domains replicate late. Across our segmented human genome, we found a high degree of covariation between mean replication timing in HUVEC cells and New SINE PC scores (Fig. 1c), new SINEs associated with early replication and new L1s associated with late replication. This result is probably not specific to HUVEC cells alone, since early and late replicating regions from various independent cell lines exhibit a high degree of overlap (Fig. S5). In addition, by splitting L1s into old and new groups, we observed a strong association between replication timing and retrotransposon age that was not reported in previous analyses (Pope et al. 2014). To confirm these results, we analysed retrotransposon accumulation at the boundaries of previously identified replication domains (RDs) (Liu et al. 2015). We focused primarily on early replicating domain (ERD) boundaries rather than late replicating domain (LRD) boundaries. ERD boundaries mark the transition from open chromatin states to closed chromatin states and overlap with topologically associated domain (TAD) boundaries (Pope et al. 2014). Consistent with our earlier results, significant density fluctuations at ERD boundaries were only observed for new L1s and new SINEs (Fig. 1c). Because RD timing and genomic distributions of clade-specific retrotransposons are both largely conserved across human and mouse (Ryba et al. 2010), these results suggest that the relationship between retrotransposon accumulation and RD timing may be conserved across mammals.

89

90

91

92

93

94

95

96

97

98

99

100

101

102

103

104

105

106

107

108

109

110

The genomic distribution of retrotransposons is conserved across species

111

112

Our results showed that the genomic distribution of retrotransposons was similar across species (Fig 1a). To determine whether our observations resulted from retrotransposon insertion into orthologous regions, we used coordinate mappings between species to humanise retrotransposon family distributions and PC scores (see methods). From this, we found that retrotransposon families in different species that identified as the same group, accumulated

113

114

115

116

117

in regions with shared common ancestry (Fig. S6-S9). In addition, humanised genome 118 segments from the 20% tails of the New SINE and Ancient PC score distributions showed 119 high degrees of genomic overlap and associated with human RDs as described above (Fig. 1b). 120 With regard to sequence conservation and retrotransposon accumulation, regions enriched 121 for ancient elements shared the highest degree of pairwise similarity across our species 122 (Fig. S10-S11). This demonstrates that regions enriched for ancient elements have likely 123 been preserved throughout mammalian evolution (Adelson et al. 2009, 2010). Our results 124 are consistent with retrotransposon accumulation overlying a conserved ancient genome 125 architecture. 126

Retrotransposon insertion in open chromatin surrounding regulatory elements 127

128

Retrotransposons preferentially insert into open chromatin, yet open chromatin usually 129 overlaps gene regulatory elements. As stated above, this creates a fundamental evolutionary 130 conflict for retrotransposons: their immediate replication may be costly to the overall fitness 131 of the genome in which they reside. To investigate retrotransposon insertion/accumulation 132 dynamics at open chromatin regions, we analysed DNase1 hypersensitive activity across 15 133 cell lines in both ERDs and LRDs. DNase1 hypersensitive sites obtained from the UCSC 134 genome browser (Consortium et al. 2012) were merged into DNase1 clusters and DNase1 135 clusters overlapping exons were excluded. As replication is sometimes cell type-specific we 136 also constructed a set of constitutive ERDs and LRDs (cERDs and cLRDs) (see methods). 137 Based on previous analyses, cERDs and cLRDs likely capture RD states present during 138 developmental periods of heritable retrotransposition (Rivera-Mulia et al. 2015). Our cERDs 139 and cLRDs capture approximately 50% of the genome and contain regions representative 140 of genome-wide intron and intergenic genome structure (Fig. S12). In both cERDs and 141 cLRDs, we measured DNase1 cluster activity by counting the number of DNase1 peaks that 142 overlapped each cluster. We found that DNase1 clusters in cERDs were much more active 143 than DNase1 clusters in cLRDs (Fig. 2a). Next, we analysed retrotransposon accumulation 144 both within and at the boundaries of DNase1 clusters. Consistent with disruption of gene 145 regulation by retrotransposon insertion, non-ancient retrotransposon groups were depleted 146 from DNase1 clusters (Fig. 2b). Intriguingly, ancient element density in DNase1 clusters 147

remained relatively high, suggesting that some ancient elements may have been exapted. At 148
DNase1 cluster boundaries after removing interval size bias (Fig. S13-S14) (see methods), 149
retrotransposon density remained highly enriched in cERDs and close to expected levels in 150
cLRDs (Fig. 2c). This suggests that chromatin is likely to be open at highly active cluster 151
boundaries where insertion of retrotransposons is less likely to disrupt regulatory elements. 152
These results are consistent with an interaction between retrotransposon insertion, open 153
chromatin and regulatory activity, where insertions into open chromatin only persist if they 154
do not interrupt regulatory elements. 155

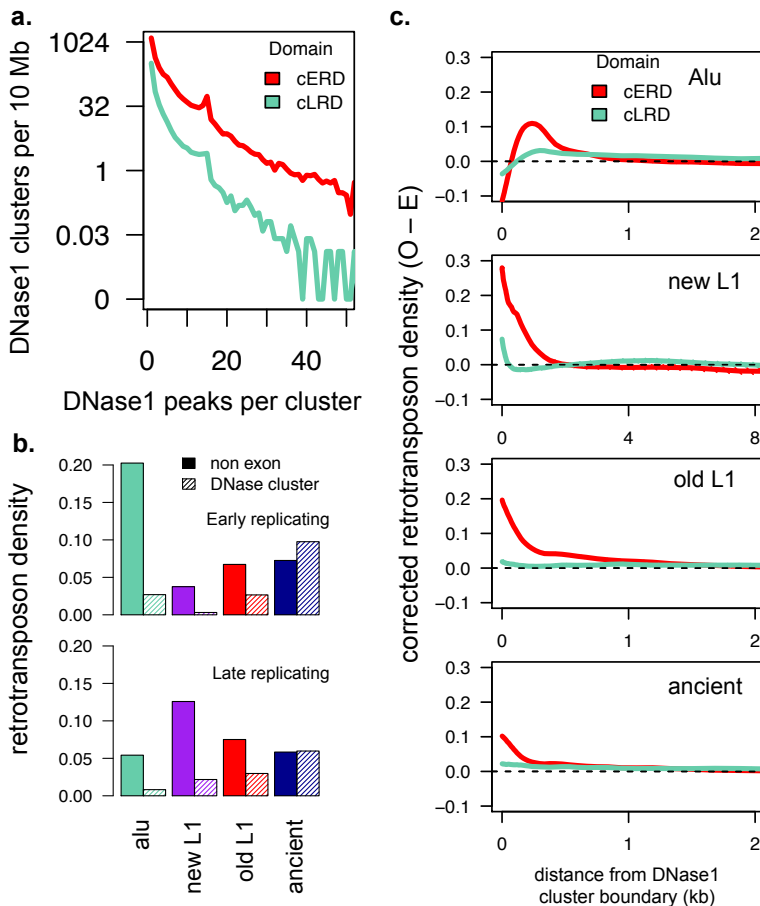


Figure 2. Retrotransposon accumulation occurs in open chromatin near regulatory regions. **a**, The activity of DNase1 clusters in cERDs and cLRDs. DNase1 clusters were identified by merging DNase1 hypersensitive sites across 15 tissues. Their activity levels were measured by the number of DNase1 hypersensitive sites overlapping each DNase1 cluster. **b**, Retrotransposon density of non-exonic regions and DNase1 clusters in cERDs and cLRDs. **c**, Observed minus expected retrotransposon density at the boundary of DNase1 clusters corrected for interval size bias (see methods). Expected retrotransposon density was calculated as each group's non-exonic total retrotransposon density across cERDs and cLRDs. A confidence interval of 3 standard deviations from expected retrotransposon density was also calculated, however the level of variation was negligible.

Retrotransposon insertion size and regulatory element density

156

L1s and their associated SINEs differ in size by an order of magnitude, retrotranspose via the L1-encoded chromatin sensitive L1ORF2P and accumulate in compositionally distinct genomic domains (Cost et al. 2001; Baillie et al. 2011). This suggests that retrotransposon insertion size determines observed accumulation patterns. L1 and *Alu* insertions occur via target-primed reverse transcription which is initiated at the 3' end of each element. With L1

157

158

159

160

161

insertion, this process often results in 5' truncation, causing extensive insertion size variation ¹⁶²
and an over representation of new L1 3' ends, not seen with *Alu* elements (Fig. 3a). When we ¹⁶³
compared insertion size variation across cERDs and cLRDs we observed that smaller new L1s ¹⁶⁴
were enriched in cERDs and *Alu* elements showed no RD insertion size preference (Fig. 3b). ¹⁶⁵
The effect of insertion size on retrotransposon accumulation was estimated by comparing ¹⁶⁶
insertion rates of each retrotransposon group at DNase1 cluster boundaries in cERDs and ¹⁶⁷
cLRDs. We found that *Alu* insertion rates at DNase1 cluster boundaries were similarly ¹⁶⁸
above expected levels both in cERDs and cLRDs (Fig. 3c), whereas new L1 insertion rates ¹⁶⁹
at DNase1 cluster boundaries were further above expected levels in cERDs than cLRDs (Fig. ¹⁷⁰
3d). By comparing the insertion rate of new L1s — retrotransposons that exhibited RD ¹⁷¹
specific insertion size variation — we found a negative correlation between element insertion ¹⁷²
size and gene/regulatory element density. Thus smaller elements, such as *Alu* elements, ¹⁷³
accumulate more in cERDs than do larger elements, such as new L1s, suggesting that smaller ¹⁷⁴
elements are more tolerated. ¹⁷⁵

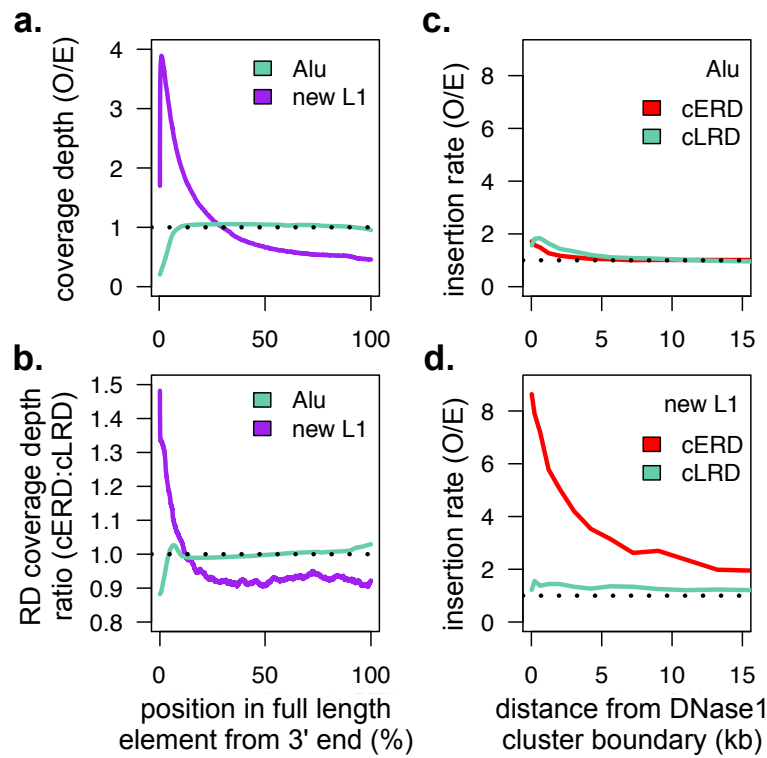


Figure 3. Retrotransposon insertion size is inversely proportional to local regulatory element density. **a**, Observed to expected ratio of retrotransposon position coverage depth measured from consensus 3' end. Expected retrotransposon position coverage depth was calculated as total retrotransposon coverage over consensus element length. We used 6 kb as the consensus new L1 length and 300 bp as the consensus *Alu* length. **b**, New L1 and *Alu* position density ratio (cERDs:cLRDs). **c**, *Alu* and **d**, new L1 observed over expected retrotransposon insertion rates at DNase1 cluster boundaries in cERDs and cLRDs. Insertion rates were measured by prevalence of 3' ends and expected levels were calculated as the per Mb insertion rate across cERDs and cLRDs.

Retrotransposon insertion within gene and exon structures

Regulatory element organisation is largely shaped by gene and exon/intron structure which likely impacts the retrotransposon component of genome architecture. Therefore, we analysed retrotransposons and DNase1 clusters (exon overlapping and not exon overlapping) at the boundaries of genes and exons. Human RefSeq gene models were obtained from the UCSC genome browser and both intergenic and intronic regions were extracted (Table S4). At gene (Fig. 4a) and exon (Fig. 4b) boundaries, we found a high density of exon overlapping DNase1 clusters and depletion of retrotransposons. This created a depleted retrotransposon boundary zone (DRBZ) specific for each retrotransposon group, a region extending from the gene or exon boundary to the point where retrotransposon levels begin to increase. The size of each

176

177

178

179

180

181

182

183

184

185

DRBZ correlated with the average insertion size of each retrotransposon group, suggesting 186
larger retrotransposons may have a greater capacity to disrupt important structural and 187
regulatory genomic features. We also found that in cERDs the 5' gene boundary *Alu* 188
DRBZ was larger than the 3' gene boundary *Alu* DRBZ. This difference was associated with 189
increased exon overlapping DNase1 cluster density at 5' gene boundaries in cERDs 190
(Fig. 4a), emphasising the importance of evolutionary constraints on promoter architecture. For 191
ancient elements, their interval size corrected density approximately 1 kb from the 5' gene 192
boundary was significantly higher than expected. This increase is consistent with exaptation 193
of ancient elements into regulatory roles (Lowe et al. 2007) (Fig. S15-S18). Moreover, the 194
density peak corresponding to uncorrected ancient elements also overlapped with that of 195
not exon overlapping DNase1 clusters (Fig. 4a). Collectively, these results demonstrate the 196
evolutionary importance of maintaining gene structure and regulation and how this in turn 197
has canalised similar patterns of accumulation and distribution of retrotransposon families 198
in different species over time. 199

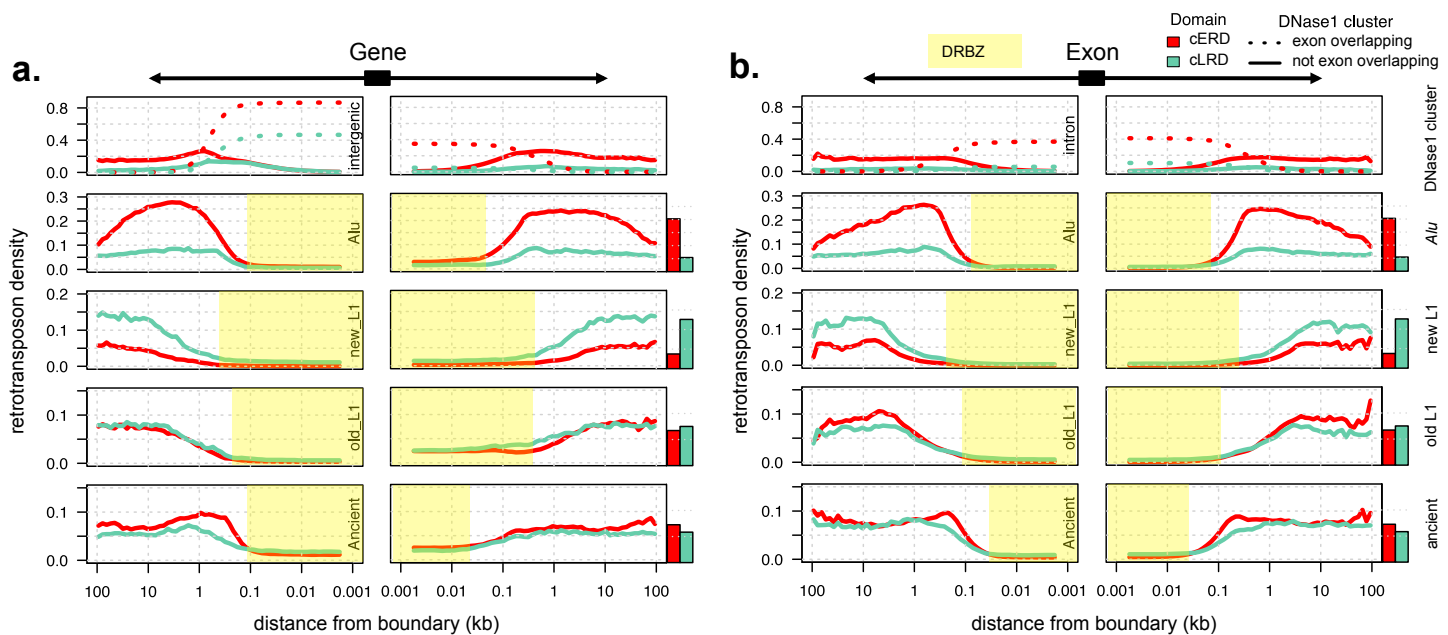


Figure 4. Retrotransposon accumulation within intergenic and intronic regions correlates with the distribution of DNase1 clusters. Density of DNase1 clusters and retrotransposons at each position upstream and downstream of genes and exons in **a**, intergenic and **b**, intronic regions. For DNase1 clusters, dotted lines represent exon overlapping clusters and solid lines represent not exon overlapping clusters. For retrotransposons, solid lines represent the uncorrected retrotransposon density at exon and gene boundaries. Bar plots show expected retrotransposon density across cERDs and cLRDs. Highlighted regions outline DRBZs, regions extending from the gene or exon boundary to the point where retrotransposon levels begin to increase.

Discussion

200

In our study, we compared several mammalian genomes and analysed chromatin structure 201 at both small and large scales to better characterise retrotransposon accumulation. Our 202 genome-wide comparisons across species were consistent with previous analyses that reported 203 high levels of positional conservation for L1s and their associated SINEs (Chinwalla et al. 204 2002; Gibbs et al. 2004). Because new L1s and new SINEs underwent periods of activity 205 after each of our sample species diverged from a common ancestor (Giordano et al. 2007), our 206 observations are likely the result of a conserved interaction between retrotransposon activity 207 and genome architecture. Previous analyses have attempted to capture this interaction 208 through various retrotransposon accumulation models (Lander et al. 2001). Based on large- 209 scale conservation of genome architecture and GC content (Chinwalla et al. 2002; Gibbs et al. 210 2004), the current model of retrotransposon accumulation suggests that random insertion 211 of L1s and SINEs are similarly constrained by local sequence composition, where L1s are 212 quickly purged from gene-rich regions via purifying selection at a higher rate than SINEs 213 (Graham and Boissinot 2006; Gasior et al. 2007; Kvikstad and Makova 2010). However, this 214 model fails to account for the demonstrated impact of chromatin structure on insertion site 215 preference (Cost et al. 2001; Baillie et al. 2011). 216

We used publicly available datasets to analyze the impact of chromatin architecture on 217 retrotransposon accumulation. However, this approach is not without its limitations. For 218 example, heritable retrotransposon insertions typically occur during embryogenesis or within 219 the germline; developmental stages and tissue samples that were unavailable. To overcome 220 such limitations we aggregated data from a range of biological contexts. Using this strategy, 221 we increased the probability of capturing chromosomal domain structures and regulatory 222 element sites present in embryonic and germline cell states. 223

From our analysis we found that 1) following preferential insertion into open chromatin 224 domains, retrotransposons were tolerated adjacent to regulatory elements where they were 225 less likely to cause harm; 2) element insertion size was a key factor affecting retrotransposon 226 accumulation, where large elements accumulated in gene poor regions where they were less 227 likely to perturb gene regulation; and 3) insertion patterns surrounding regulatory elements 228 were persistent at the gene level. Based on these results, we propose a significant change to 229 the current retrotransposon accumulation model; rather than random insertion constrained 230

by local sequence composition, we propose that insertion is instead primarily constrained 231
by local chromatin structure. Following this, L1s and SINEs both preferentially insert into 232
gene/regulatory element rich euchromatic domains, where L1s with their relatively high 233
mutational burden are quickly eliminated via purifying selection at a much higher rate than 234
SINEs. Over time this results in an enrichment of SINEs in euchromatic domains and an 235
enrichment of L1s in heterochromatic domains. 236

In conjunction with large scale conservation of synteny (Chowdhary et al. 1998), gene 237
regulation (Chan et al. 2009) and the structure of RDs/TADs (Dixon et al. 2012; Ryba et al. 238
2010), our findings suggest that large scale positional conservation of old and new non-LTR 239
retrotransposons results from their association with the regulatory activity of large genomic 240
domains. From this, we conclude that similar constraints on insertion and accumulation of 241
retrotransposons in different species can define common trajectories for genome evolution. 242

Methods 243

Within species comparisons of retrotransposon genome distributions 244

Retrotransposon coordinates for each species were initially identified using RepeatMasker 245
and obtained from UCSC genome browser (Table S1) (Smit et al. 1996; Rosenbloom et al. 246
2015). We grouped retrotransposon elements based on repeat IDs used in Giordano *et* 247
al (Giordano et al. 2007). Retrotransposon coordinates were extracted from hg19, mm9, 248
panTro4, rheMac3, and canFam3 assemblies. Each species genome was segmented into 1 249
Mb regions and the density of each retrotransposon family for each segment was calculated. 250
From this, each species was organised into an n -by- p data matrix of n genomic segments and 251
 p retrotransposon families. Genome distributions of retrotransposons were then analysed 252
using principle component analysis (PCA) and correlation analysis. For correlation analysis, 253
for each retrotransposon family we calculated Pearson's correlation coefficient for each 254
retrotransposon family across our genome segments. 255

Across species comparisons of retrotransposon genome distributions 256

To compare genome distributions across species, we humanised a query species genome using 257
mapping coordinates extracted from net AXT alignment files located on the UCSC genome 258
browser (Table S1). First, genomes were filtered by discarding segments below a minimum 259

mapping fraction threshold, removing poorly represented regions (Fig S19a). Next, we used 260
mapping coordinates to match fragments of query species segments to their corresponding 261
human segments (Fig S19b). From this, the retrotransposon content and PC scores of the 262
matched query segments were humanised following equation 1 (Fig S19c). 263

$$c_i^* = \frac{\sum_j c_{ij} l_j^Q / q_j}{\sum_j l_j^R / r}, \quad (1)$$

where c_{ij} is the density of retrotransposon family i in query segment j , l_j^Q is the total length 264
of the matched fragments between query segment j and the reference segment, l_j^R is the total 265
length of the reference segment fragments that match query segment j , q_j is the total length 266
of the query segment j , and r is the total length of the reference segment. The result c_i^* is 267
the humanised coverage fraction of retrotransposon family i that can now be compared to a 268
specific reference segment. Once genomes were humanised, Pearson's correlation coefficient 269
was used to determine the conservation between retrotransposon genomic distributions 270
(Fig S19d). Using the Kolmogorov-Smirnov test, we measured the effect of humanising by 271
comparing the humanised query retrotransposon density distribution to the query filtered 272
retrotransposon density distribution (Fig S19e). The same was done to measure the effect 273
of filtering by comparing the segmented human retrotransposon density distribution to the 274
human filtered retrotransposon density distribution (Fig S19f). Spatial correlations and 275
the P-values from measuring the effects of humanising and filtering were integrated into a 276
heatmap (Fig S19g). The entire process was repeated several times at different minimum 277
mapping fraction thresholds to optimally represent each retrotransposon families genomic 278
distribution in a humanised genome (fig S20). 279

Replication timing boundaries and constitutive replication timing domains 280

ERDs, LRDs, and timing transition regions (TTRs) for each dataset were previously identified 281
using a deep neural network hidden Markov model (Table S2) (Liu et al. 2015). To determine 282
RD boundary fluctuations of retrotransposon density, we defined ERD boundaries as the 283
boundary of a TTR adjacent to an ERD. ERD boundaries from across each sample were 284
pooled and retrotransposon density was calculated for 50 kb intervals from regions flanking 285
each boundary 1 Mb upstream and downstream. Expected density and standard deviation 286
for each retrotransposon group was derived from a background distribution generated by 287

calculating the mean of 500 randomly sampled 50 kb genomic bins within 2000 kb of each 288
ERD boundary, replicated 10000 times. We also obtained Repli-Seq replication timing 289
profiles from the UCSC genome browser as a wavelet signal (Table S2) (Hansen et al. 2010b). 290
For each of our 50 kb intervals we calculated the mean replication timing from across each 291
Repli-Seq sample. To identify cERDs and cLRDs, ERDs and LRDs classified by Liu *et al* 292
(Liu et al. 2015) across each cell type were split into 1 kb intervals to find the intersection. If 293
the classification of 12 out of 16 samples agreed at a certain region, we classified that region 294
as belonging to a cERDs or a cLRDs, depending on that region's majority classification. 295

DNase1 cluster identification and activity 296

DNase1 sites across 15 cell lines were found using DNase-seq and DNase-chip as part of the 297
open chromatin synthesis dataset for ENCODE (Table S3) (Consortium et al. 2012). Regions 298
where P-values of contiguous base pairs were below 0.05 were identified as significant DNase1 299
hypersensitive sites (Consortium et al. 2012). From this we extracted significant DNase1 300
hypersensitive sites from each sample and pooled them. DNase1 hypersensitive sites were 301
then merged into DNase1 clusters. Cluster activity was calculated as the number of total 302
overlapping pooled DNase1 hypersensitive sites. We also extracted intervals between adjacent 303
DNase1 clusters to look for enrichment of retrotransposons at DNase1 cluster boundaries. 304

Extraction of intergenic and intron intervals 305

hg19 RefSeq gene annotations obtained from UCSC genome browser were used to extract 306
a set of introns and intergenic intervals (Table S4). RefSeq gene annotations were merged 307
and intergenic regions were classified as regions between the start and end of merged gene 308
models. We used the strandedness of gene model boundaries to classify adjacent intergenic 309
region boundaries as upstream or downstream. We discarded intergenic intervals adjacent 310
to gene models where gene boundaries were annotated as both + and - strand. Regions 311
between adjacent RefSeq exons within a single gene model were classified as introns. Introns 312
interrupted by exons in alternatively spliced transcripts and introns overlapped by other gene 313
models were excluded. Upstream and downstream intron boundaries were then annotated 314
depending on the strandedness of the gene they were extracted from. 315

Interval boundary density of retrotransposons

316

Intervals were split in half and positions were reckoned relative to the feature adjacent 317 boundary, where the feature was either a gene, exon, or DNase1 cluster (Fig S21). To 318 calculate the retrotransposon density at each position, we measured the fraction of bases at 319 each position annotated as a retrotransposon. Next, we smoothed retrotransposon densities 320 by calculating the mean and standard deviation of retrotransposon densities within an 321 expanding window, where window size grew as a function of distance from the boundary as 322 position depth decreased. This made it possible to accurately compare the retrotransposon 323 density at positions where retrotransposon insertions were sparse and density levels at 324 each position fluctuated drastically. At positions with a high base pair density a small 325 window was used and at positions with a low base pair density a large window was used. 326 Expected retrotransposon density p was calculated as the total proportion of bases covered 327 by retrotransposons across all intervals. Standard deviation at each position was calculated 328 as \sqrt{npq} , where n is the total number of bases at a given position and q is equal to $1 - p$. 329

Interval size bias correction of retrotransposon densities

330

Interval boundary density is sensitive to retrotransposon insertion preferences into intervals 331 of a certain size (Fig S22). To determine interval size retrotransposon density bias, we 332 grouped intervals according to size and measured the retrotransposon density of each interval 333 size group. Retrotransposon density bias was calculated as the observed retrotransposon 334 density of an interval size group divided by the expected retrotransposon density, where the 335 expected retrotransposon density is the total retrotransposon density across all intervals. 336 Next, using the intervals that contribute to the position depth at each position adjacent 337 to feature boundaries, we calculated the mean interval size. From this we corrected retro- 338 transposon density at each position by dividing the observed retrotransposon density by the 339 retrotransposon density bias that corresponded with that position's mean interval size. 340

Software and data analysis

341

All statistical analyses were performed using R (R Core Team 2015) with the packages 342 GenomicRanges (Lawrence et al. 2013) and rtracklayer (Lawrence et al. 2009). R scripts 343 used to perform analyses can be found at: 344

<https://github.com/AdelaideBioinfo/retrotransposonAccumulation> .

345

Additional Files

346

Additional file 1 — Supplementary information

347

Figures S1–S22, Tables S1–S4.

348

Competing interests

349

The authors declare that they have no competing interests.

350

Author's contributions

351

R.M.B., R.D.K., J.M.R., and D.L.A. designed research; R.M.B. performed research; and 352
R.M.B., R.D.K., and D.L.A. wrote the paper. 353

Acknowledgements

354

For reviewing our manuscript and providing helpful advice we would like to thank the 355
following: Simon Baxter, Atma Ivancevic and Lu Zeng from the University of Adelaide; 356
Kirsty Kitto from Queensland University of Technology; and Udaya DeSilva from Oklahoma 357
State University. 358

Availability of data and materials

359

All data was obtained from publicly available repositories, urls can be found in sup- 360
porting material (Table S1–S3). R scripts used to perform analyses can be found at 361
<https://github.com/AdelaideBioinfo/retrotransposonAccumulation>. 362

References

Adelson, D., Raison, J., Garber, M., and Edgar, R. (2010). Interspersed repeats in the horse
(*equus caballus*); spatial correlations highlight conserved chromosomal domains. *Animal*
genetics, 41(s2):91–99.

Adelson, D. L., Raison, J. M., and Edgar, R. C. (2009). Characterization and distribution of retrotransposons and simple sequence repeats in the bovine genome. *Proceedings of the National Academy of Sciences*, 106(31):12855–12860.

Ashida, H., Asai, K., and Hamada, M. (2012). Shape-based alignment of genomic landscapes in multi-scale resolution. *Nucleic acids research*, 40(14):6435–6448.

Baillie, J. K., Barnett, M. W., Upton, K. R., Gerhardt, D. J., Richmond, T. A., De Sapi, F., Brennan, P. M., Rizzu, P., Smith, S., Fell, M., et al. (2011). Somatic retrotransposition alters the genetic landscape of the human brain. *Nature*, 479(7374):534–537.

Bao, W., Kojima, K. K., and Kohany, O. (2015). Repbase update, a database of repetitive elements in eukaryotic genomes. *Mobile DNA*, 6(1):1.

Chalopin, D., Naville, M., Plard, F., Galiana, D., and Volff, J.-N. (2015). Comparative analysis of transposable elements highlights mobilome diversity and evolution in vertebrates. *Genome biology and evolution*, 7(2):567–580.

Chan, E. T., Quon, G. T., Chua, G., Babak, T., Trochesset, M., Zirngibl, R. A., Aubin, J., Ratcliffe, M. J., Wilde, A., Brudno, M., et al. (2009). Conservation of core gene expression in vertebrate tissues. *Journal of biology*, 8(3):1.

Chinwalla, A. T., Cook, L. L., Delehaunty, K. D., Fewell, G. A., Fulton, L. A., Fulton, R. S., Graves, T. A., Hillier, L. W., Mardis, E. R., McPherson, J. D., et al. (2002). Initial sequencing and comparative analysis of the mouse genome. *Nature*, 420(6915):520–562.

Chowdhary, B. P., Raudsepp, T., Frönicke, L., and Scherthan, H. (1998). Emerging patterns of comparative genome organization in some mammalian species as revealed by zoo-fish. *Genome research*, 8(6):577–589.

Consortium, E. P. et al. (2012). An integrated encyclopedia of dna elements in the human genome. *Nature*, 489(7414):57–74.

Cost, G. J., Feng, Q., Jacquier, A., and Boeke, J. D. (2002). Human l1 element target-primed reverse transcription in vitro. *The EMBO Journal*, 21(21):5899–5910.

Cost, G. J., Golding, A., Schlissel, M. S., and Boeke, J. D. (2001). Target dna chromatinization modulates nicking by l1 endonuclease. *Nucleic acids research*, 29(2):573–577.

Dixon, J. R., Selvaraj, S., Yue, F., Kim, A., Li, Y., Shen, Y., Hu, M., Liu, J. S., and Ren, B. (2012). Topological domains in mammalian genomes identified by analysis of chromatin interactions. *Nature*, 485(7398):376–380.

Furano, A. V., Duvernall, D. D., and Boissinot, S. (2004). L1 (line-1) retrotransposon diversity differs dramatically between mammals and fish. *Trends in Genetics*, 20(1):9–14.

Gasior, S. L., Preston, G., Hedges, D. J., Gilbert, N., Moran, J. V., and Deininger, P. L. (2007). Characterization of pre-insertion loci of de novo l1 insertions. *Gene*, 390(1):190–198.

Gibbs, R. A., Weinstock, G. M., Metzker, M. L., Muzny, D. M., Sodergren, E. J., Scherer, S., Scott, G., Steffen, D., Worley, K. C., Burch, P. E., et al. (2004). Genome sequence of the brown norway rat yields insights into mammalian evolution. *Nature*, 428(6982):493–521.

Gibcus, J. H. and Dekker, J. (2013). The hierarchy of the 3d genome. *Molecular cell*, 49(5):773–782.

Giordano, J., Ge, Y., Gelfand, Y., Abrusán, G., Benson, G., and Warburton, P. E. (2007). Evolutionary history of mammalian transposons determined by genome-wide defragmentation. *PLoS Comput Biol*, 3(7):e137.

Graham, T. and Boissinot, S. (2006). The genomic distribution of l1 elements: the role of insertion bias and natural selection. *BioMed Research International*, 2006.

Hansen, R. S., Thomas, S., Sandstrom, R., Canfield, T. K., Thurman, R. E., Weaver, M., Dorschner, M. O., Gartler, S. M., and Stamatoyannopoulos, J. A. (2010a). Sequencing newly replicated dna reveals widespread plasticity in human replication timing. *Proceedings of the National Academy of Sciences*, 107(1):139–144.

Hansen, R. S., Thomas, S., Sandstrom, R., Canfield, T. K., Thurman, R. E., Weaver, M., Dorschner, M. O., Gartler, S. M., and Stamatoyannopoulos, J. A. (2010b). Sequencing newly replicated dna reveals widespread plasticity in human replication timing. *Proceedings of the National Academy of Sciences*, 107(1):139–144.

Kramerov, D. and Vassetzky, N. (2011). Origin and evolution of sines in eukaryotic genomes. *Heredity*, 107(6):487–495.

Kvikstad, E. M. and Makova, K. D. (2010). The (r) evolution of sine versus line distributions in primate genomes: sex chromosomes are important. *Genome research*, 20(5):600–613.

Lander, E. S., Linton, L. M., Birren, B., Nusbaum, C., Zody, M. C., Baldwin, J., Devon, K., Dewar, K., Doyle, M., FitzHugh, W., et al. (2001). Initial sequencing and analysis of the human genome. *Nature*, 409(6822):860–921.

Lawrence, M., Gentleman, R., and Carey, V. (2009). rtracklayer: an r package for interfacing with genome browsers. *Bioinformatics*, 25:1841–1842.

Lawrence, M., Huber, W., Pagès, H., Aboyoun, P., Carlson, M., Gentleman, R., Morgan, M., and Carey, V. (2013). Software for computing and annotating genomic ranges. *PLoS Computational Biology*, 9.

Liu, F., Ren, C., Li, H., Zhou, P., Bo, X., and Shu, W. (2015). De novo identification of replication-timing domains in the human genome by deep learning. *Bioinformatics*, page btv643.

Lowe, C. B., Bejerano, G., and Haussler, D. (2007). Thousands of human mobile element fragments undergo strong purifying selection near developmental genes. *Proceedings of the National Academy of Sciences*, 104(19):8005–8010.

Medstrand, P., Van De Lagemaat, L. N., and Mager, D. L. (2002). Retroelement distributions in the human genome: variations associated with age and proximity to genes. *Genome research*, 12(10):1483–1495.

Murphy, W. J., Larkin, D. M., Everts-van der Wind, A., Bourque, G., Tesler, G., Auvil, L., Beever, J. E., Chowdhary, B. P., Galibert, F., Gatzke, L., et al. (2005). Dynamics of mammalian chromosome evolution inferred from multispecies comparative maps. *Science*, 309(5734):613–617.

Pope, B. D., Ryba, T., Dileep, V., Yue, F., Wu, W., Denas, O., Vera, D. L., Wang, Y., Hansen, R. S., Canfield, T. K., et al. (2014). Topologically associating domains are stable units of replication-timing regulation. *Nature*, 515(7527):402–405.

R Core Team (2015). *R: A Language and Environment for Statistical Computing*. R Foundation for Statistical Computing, Vienna, Austria.

Rivera-Mulia, J. C., Buckley, Q., Sasaki, T., Zimmerman, J., Didier, R. A., Nazor, K., Loring, J. F., Lian, Z., Weissman, S., Robins, A. J., et al. (2015). Dynamic changes in replication timing and gene expression during lineage specification of human pluripotent stem cells. *Genome research*.

Rosenbloom, K. R., Armstrong, J., Barber, G. P., Casper, J., Clawson, H., Diekhans, M., Dreszer, T. R., Fujita, P. A., Guruvadoo, L., Haeussler, M., et al. (2015). The ucsc genome browser database: 2015 update. *Nucleic acids research*, 43(D1):D670–D681.

Ryba, T., Hiratani, I., Lu, J., Itoh, M., Kulik, M., Zhang, J., Schulz, T. C., Robins, A. J., Dalton, S., and Gilbert, D. M. (2010). Evolutionarily conserved replication timing profiles predict long-range chromatin interactions and distinguish closely related cell types. *Genome research*, 20(6):761–770.

Smit, A. F., Hubley, R., and Green, P. (1996). Repeatmasker open-3.0.